



Efficient photocatalytic degradation of tetracycline in wastewater with non-layered 2D PbMoO₄

Zhengping He^a, Yaohui Wu^{a,*}, Zhenggang Xu^a, Xinjiang Hu^b, Yonghong Wang^a, Gaoqiang Liu^a, Yunlin Zhao^{a,*}

^aCollege of Life Science and Technology, Central South University of Forestry and Technology, Changsha 410004, China, emails: wyh752100@163.com (Y.H. Wu), 15673775866@163.com (Z.P. He), 5673775866@163.com (Z.G. Xu), bionano@163.com (Y.H. Wang), gaoliuedu@yahoo.com.cn (G.Q. Liu), zyl8291290@163.com (Y.L. Zhao)

^bCollege of Environmental Science and ENGINEERING, Central South University of Forestry and Technology, Changsha 410004, China, email: xjhu@csuft.edu.cn (X.H. Hu)

Received 19 December 2019; Accepted 29 August 2020

ABSTRACT

In this study, a photocatalyst, non-layered 2D lead molybdate nanoparticles (2D PbMoO₄), was obtained by ultrasonic stripping and dipping pulling methods and applied to photocatalytic degradation of tetracycline (TC) in wastewater. The two-dimensional morphology and body-centered tetragonal structure of 2D PbMoO₄ were ascertained by atomic force microscopy, X-ray diffraction and transmission electron microscopy. The bandgap and chemical environment of 2D PbMoO₄ had been ascertained by UV-Vis and X-ray photoelectron spectroscopy analysis. Photoelectrochemical measurement experiments were used to evaluate the charge separation efficiency and charge transfer process of 2D PbMoO₄. The effects of some factors in the photocatalytic conditions including 2D PbMoO₄ dosage, pH and initial TC concentration on the degradation were investigated. The degradation efficiency of TC in different water matrix was obtained utilizing ultrapure water (UW), artificial wastewater (AW), farm wastewater (FW) and municipal wastewater (MW). The removal rate of TC in UW, AW, FW and MW was 96%, 94%, 91% and 88%, respectively. In UW, the degradation of TC exhibited the highest rate constant (0.01977, $R^2 = 0.99447$), followed by that obtained in AW (0.01706, $R^2 = 0.97692$), FW (0.01543, $R^2 = 0.99692$) and MW (0.01367, $R^2 = 0.98584$). Additionally, 2D PbMoO₄ showed high recyclability and stability. After five recycling performance, there was still 95% of TC were eliminated. The first-order kinetic model was used to simulate the photocatalytic degradation of TC in the four kinds of wastewater. The work indicated that 2D PbMoO₄ had promising potential for antibiotic-containing wastewater treatment.

Keywords: Photocatalyst; 2D PbMoO₄; Tetracycline; Wastewater

1. Introduction

Since the advent of tetracycline in 1948, it had been widely used in clinical treatment and farm prevention due to their low-cost, ease of use, and low side effects [1,2]. At present, different concentrations of tetracycline (TC) antibiotic residues had been detected in samples of farm manure,

farmland soil and rivers. A high level of TC had been detected in Huangpu River Basin and Pearl River Delta in China, ranging from 53.5 ng L⁻¹ to 16 µg L⁻¹ [3,4]. TC and a large number of organic pollutants were detected in 139 major rivers in the United States [5]. The average level of TC in surface and groundwater resources near animal farms in Tehran, Iran was between 5.4–8.1 ng L⁻¹ [6]. In the analysis

* Corresponding authors.

of effluent from waste-water treatment plants in hospitals and pharmaceutical factories in India, extremely high concentrations (mg L^{-1} range) broad-spectrum antibiotics were detected.

The unmetabolized TC in the environment that acted as an external factor, breaking the original biological environment and indirectly endangering human health. The environment with low concentration levels of TC could induce genetic mutations in bacteria, resulting in the formation of TC resistant bacteria [7]. TC affected its growth and development by inhibiting enzymes in animals and plants [8,9]. In addition, TC residues in the food pose a potential risk to human health affected the normal growth and development of the human body, leading to liver and kidney poisoning, hemolytic anemia, discoloration of teeth, nails and sclera [10,11]. More seriously, it was easy to enter the fetus through the placenta and cause fetal malformation due to their high biological activity [12]. Therefore, it was of great significance to conduct a comprehensive study to develop novel, efficient and sustainable technologies for removing TC and their derivatives from the environment.

Traditional methods, such as physical adsorption and biodegradation, couldn't remove TC effectively from wastewater [13,14]. Currently, the use of photocatalysis to efficiently degrade TC was a hot topic for environmentalists [15,16]. Photocatalysis degradation technology was that semiconductors produce strong oxidizing free radicals under the excitation of light, which could convert contaminants into simple and nontoxic molecules, such as (hydroxyl radical (OH^{\bullet}), sulfate radical ($\text{SO}_4^{\bullet-}$) and superoxide radical ($\text{O}_2^{\bullet-}$), etc.). However, the mechanisms and application of 2D PbMoO_4 photocatalytic degradation TC under sunlight need further investigation to guide engineering applications. Therefore, this paper discusses non-layered 2D PbMoO_4 which was synthesized to degrade TC in ultrapure water (UW), artificial wastewater (AW), municipal wastewater (MW), and farm wastewater (FW) under simulated sunlight. This study was mainly aimed to (1) investigate the performances of non-layered 2D PbMoO_4 catalyst for degradation of TC in wastewater, (2) evaluate the conditions for TC efficient degradation with the catalyst, (3) study the catalytic stability of non-layered 2D PbMoO_4 and determine the possible mechanism including the dominating reactive species during the photocatalytic process.

2. Materials and methods

2.1. Chemicals

TC (standard), absolute ethanol, dimethyl sulfoxide (DMSO), ethylenediaminetetraacetic acid (EDTA), isopropyl alcohol (IPA), MoO_3 , PbCl_2 , *p*-quinone; 1,4-benzoquinone (PBQ) were purchased from Shanghai Yuanye Bio-Technology Co., Ltd. The AW was prepared from glucose, sodium nitrate, potassium dihydrogen phosphate, ammonium chloride, urea and the concentrations of the components were as follows: 5 mg L^{-1} total phosphorus, 51 mg L^{-1} total nitrogen, 60 mg L^{-1} total organic carbon [17]. MW was obtained in a sewage treatment plant in Changsha (Hunan, China). FW was acquired on a farm in Changsha (Hunan China). AW, MW, and FW were filtered by using a 0.22 μm filter before use.

2.2. Synthesis of non-layered 2D PbMoO_4

MoO_3 (4 g) powder was mixed into 50 mL of ethanol solution and then treated with an ultrasonic cleaner (SB-5200DTD Scientz Beijing China) at 300 W for 120 min. Then, centrifuged at 3,000 rpm for 20 min (H/T18MM Herexi Hunan China), the superabundant was collected as it contained α -molybdenum oxide and labeled as solution A. The sample containing 1 mM PbCl_2 was prepared as solution B. 2D PbMoO_4 was achieved by mixing solution A with a small amount of solution B (1 mL of B in 8 mL of A). After centrifugation at 8,000 rpm for 20 min, the precipitate was taken as a 2D PbMoO_4 nanosheet [18,19].

2.3. Material characterization

Atomic force microscopy (AFM) was carried out using a Bruker Dimension Icon (Madison, Wisconsin, USA) AFM. X-ray photoelectron spectroscopy (XPS) was conducted on a Thermo Fisher Scientific (Escalab 250Xi, Waltham, Massachusetts, USA) instrument equipped with a monochromated Al K- α source. X-ray diffraction (XRD) patterns of the 2D nanosheets were collected using a Bruker D8 (Madison, Wisconsin, USA) with monochromatic Cu K α as a radiation source. High-resolution transmission electron microscopy was conducted on a FEI TecnaiTM G20 (Oregon, USA). The UV-Vis diffuse reflectance spectroscopy was carried out using an Agilent Cary 5000-UV/Vis/NIR (California, USA) spectrophotometer equipped with an integrating sphere. The analysis range was from 200 to 800 nm, and BaSO_4 was used as a reflectance standard.

2.4. Photoelectrochemical measurements experiments

The electrochemical experiments were conducted on a CHI660E electrochemical workstation (Shanghai Chenhua Co., China). The PbMoO_4 film electrodes on ITO served as the working electrode, while a platinum matured calomel electrode and a carbon electrode were employed as the reference electrode and counter electrode, respectively. Na_2SO_4 (0.5 M) was used as the supporting electrolyte and a power of 300 W xenon lamp acted as a visible-light source. The photocurrent response of 2D PbMoO_4 was realized using an operating voltage of 0 V at room temperature.

2.5. Photocatalytic degradation of TC

All the degradation experiments were performed in a 250 mL quartz beaker with a photochemical reactor (CEL-HXF300 Education Au-Light, Beijing, China) equipped with a 300 W xenon lamp. The desired amounts of TC were added in UW, AW, FW, and MW to prepare TC wastewater. The initial pH of the solution was regulated by the addition of 0.1 M NaOH or 0.1 M HCl. In each experiment, a certain amount of the photocatalyst was added into 50 mL of TC solution. The suspension was stirred by a magnetic stirrer, and the reaction was performed in a batch mode operation at room temperature. The influence of operational parameters was consecutively studied including irradiation time (0–120 min), 2D PbMoO_4 dosage (30–150 mg L^{-1}), initial pH (3–11) and TC concentration (50–250 mg L^{-1}).

Five cycles of photocatalytic degradation of TC were conducted in selected conditions to assess the possibility of recycling of the 2D PbMoO₄. After each run, 2D PbMoO₄ powder was collected from the TC solution by centrifugation and washing process. After five cycles, the obtained catalyst was dried for observing the XRD and XPS patterns. A specific amount solution of EDTA, DMSO, PBQ and IPA was injected into the photocatalytic reaction solution to investigate the contribution of each radical on TC degradation, respectively. After that, the high-performance liquid chromatography (HPLC) was used to detect TC concentration. All of the experiments were performed in triplicate, and the average values were used as results.

2.6. Analytical methods

The concentration of TC in wastewater was detected at 360 nm using a HPLC system (Agilent 1200, California, USA). The mobile phase was 0.05 M phosphate buffer at pH 2.3 (80%) and acetonitrile (20%) with a flow rate of 1.0 mL min⁻¹ [20]. The removal efficiency of TC was expressed using the following equation:

$$\text{Removal efficiency} = \frac{C_t}{C_0} \times 100\% \quad (1)$$

where C_0 and C_t were the concentrations of TC before and after the photocatalytic reaction, respectively.

2.7. Identification of degradation intermediates

The degradation intermediates products of TC were determined by liquid chromatography–mass spectrometry (LC-MS)/MS system. In the process of photocatalysis, samples were taken at time 0, 45, and 120 min, and centrifuged at 12,000 rpm to completely remove the photocatalyst. The centrifuged sample filtrated with a 0.45 μm Millipore filter to remove impurities. The mobile phase was a mixture of 0.1% (v/v) acetonitrile and formic acid. The elution procedure was set as follows: from 90% formic acid and 10% acetonitrile to 10% formic acid and 90% acetonitrile within 10 min and maintained 4 min. Then, the eluent quickly adjusted to 0% formic acid and 10% acetonitrile and maintain for 2 min. MS was performed by operating in the positive ionization mode using electrospray ionization, and MS was scanned by mass between m/z 200–500 [21,22].

3. Results and discussion

3.1. Characterization of 2D PbMoO₄

3.1.1. Atomic force microscopy

AFM was used to investigate the thicknesses and lateral dimensions of the 2D PbMoO₄ nanosheets. As shown in Fig. 1a, the 2D PbMoO₄ nanosheets had an average thickness (T_{average}) of ~1.5 nm. Fig. 1c reveals that the average lateral sizes (L_{average}) of 2D PbMoO₄ nanosheets were approximately 25 nm. The T_{average} and L_{average} values obtained for both 2D molybdenum oxide and 2D PbMoO₄ nanosheets also lead to aspect ratios ($L_{\text{average}}/T_{\text{average}}$) of ~ 16, which was similar to another reported values obtained for the

exfoliated 2D PbMoO₄ nanosheets using the same method [23]. The 2D sheets have a large surface area and high mechanical stiffness [24]. Moreover, as illustrated by Fig. 1b, the 2D PbMoO₄ nanosheets had step-rich surfaces, which could enhance the reaction active sites and dangling bonds.

3.1.2. X-ray diffraction

The XRD pattern of PbMoO₄ is demonstrated in Fig. 2. In the prepared 2D PbMoO₄ sample the XRD pattern was consistent with the diffraction pattern of PbMoO₄ crystal observed in the body-centered tetragonal structure (scheelite type) (JCPDS card number 44–1486) [25]. The diffraction peaks at 32.9°, 29.5°, 27.5° and 17.9° could be assigned to the (200), (004), (112) and (101) atomic planes of PbMoO₄ crystallographic phase. For the crystal arrangement of the PbMoO₄, four equivalent oxygen atoms surrounded a molybdenum atom to compose [MoO₄]²⁻ tetrahedrons which were linked via Pb²⁺ [26]. The sharp diffraction peaks and relative intensities indicated that the PbMoO₄ was well-crystallized and had an ordered structure at a long-range. The results showed that the prepared samples were all tetragonal molybdenum-lead type structures, and there was no impurity peak was observed in the XRD pattern, indicating the example had high purity.

3.1.3. X-ray photoelectron spectroscopy

The XPS was used to research the binding energies and chemical environment of the 2D PbMoO₄ nanosheets, and the results are presented in Fig. 3. Mo 3d_{5/2} peak was at 232.53 eV and Mo 3d_{3/2} peak was at 235.73 eV, Mo⁶⁺ oxidation state was existed in 2D PbMoO₄ [27]. The O 1s patterns of XPS mainly had two peaks around 530.93 and 530.38 eV. The peak 530.93 eV should correspond to Mo = O and Pb–O bonds and could be allocated to the oxygen species involved in metal oxide chemical bonds in the sample. The Pb 4f XPS spectrum of 2D PbMoO₄ (Fig. 3d) showed double peaks at 143.68 and 138.78 eV, represented Pb 4f_{5/2} and Pb 4f_{7/2}, respectively [28,29]. These peaks indicated the Pb–O bond emerging from Pb²⁺ ions of PbMoO₄ [30].

3.1.4. Transmission electron microscopy

The TEM images of the synthesized sample are shown in Fig. 4. From Figs. 4a and b (from high to low magnification) it could be obtained that the sample morphology with length from 60 to 100 nm. Fig. 4c presents that the lattice fringe spacing of the synthesized sample was 0.33 nm. Fig. 4d is an electron diffraction diagram of the prepared example, that had many bright spots indicating the PbMoO₄ was a single crystal. Based on the above results, the sample characterization of the catalyst obtained in this work was consistent with the previously reported results, suggesting it was no-layered 2D PbMoO₄ [31].

3.1.5. Ultraviolet–visible

The bandgap of the 2D nanosheets was determined by integrating sphere supported UV-Vis spectroscopy. As Fig. 5a shows because the 2D PbMoO₄ nanosheet had a wider bandgap, absorbance started from a lower wavelength

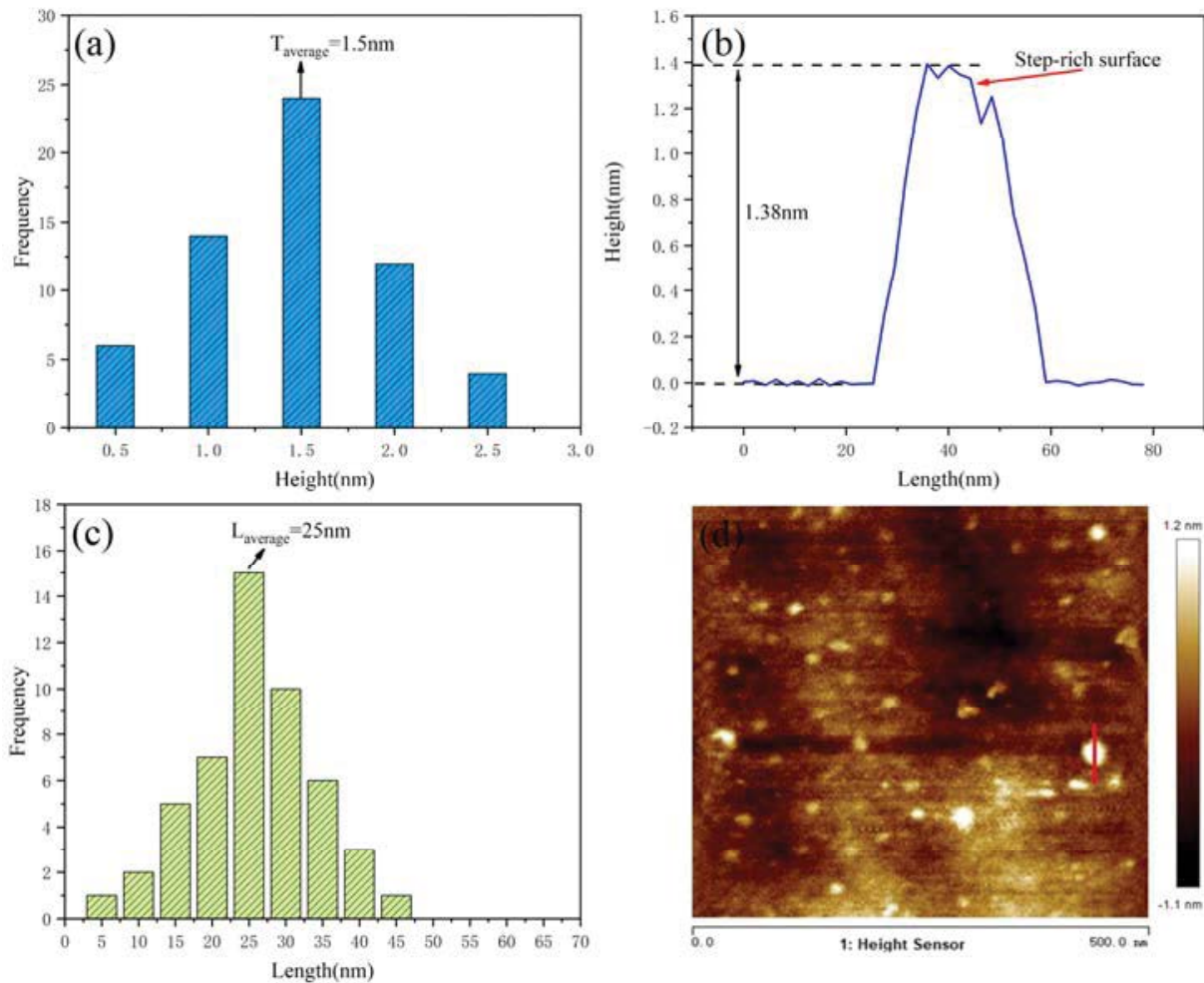


Fig. 1. AFM characterization of the 2D PbMoO_4 , (a) frequency histogram of the observed thickness, (b) corresponding thickness profile, (c) frequency histogram of the observed lateral sizes, and (d) AFM image of the nanosheet.

region at 380 nm. It had been suggested that molybdate had a direct band structure [30]. Here the band gap value of the 2D PbMoO_4 nanosheet was calculated to be 1.93 eV by the following formula:

$$(\alpha h\nu)^2 = A(h\nu - E_g)^n \quad (2)$$

where E_g was the bandgap, A was a proportionality constant, $h\nu$ was photon energy, and α was an optical absorption coefficient. As Fig. 5b shows the XPS valence band (VB) spectrum revealed that the VB position for 2D PbMoO_4 resides at 3.3 eV. The trap states in the XPS VB spectrum of 2D PbMoO_4 nanosheets could be observed, which were caused by oxygen vacancies [32]. The existence of trap states effectively reduces the bandgap of 2D PbMoO_4 and effectively shifted the photo-response towards the visible range.

3.1.6. Photocurrent measurement

Among the experimental conditions under visible light irradiation, the critical factor for the photocatalyst to

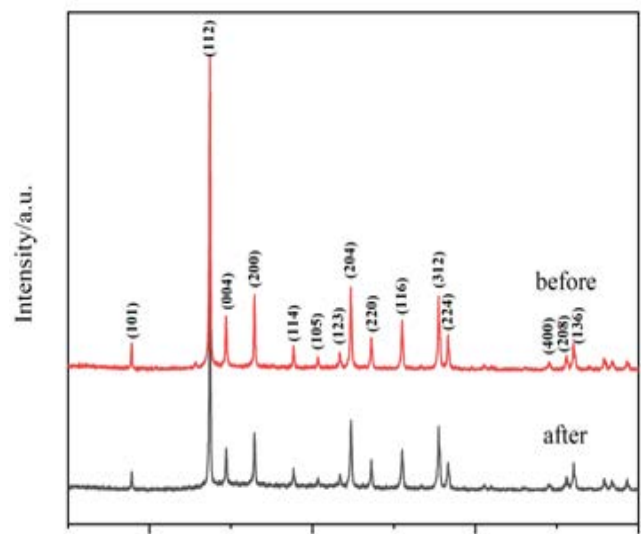


Fig. 2. XRD spectra for the catalyst before and after used five times.

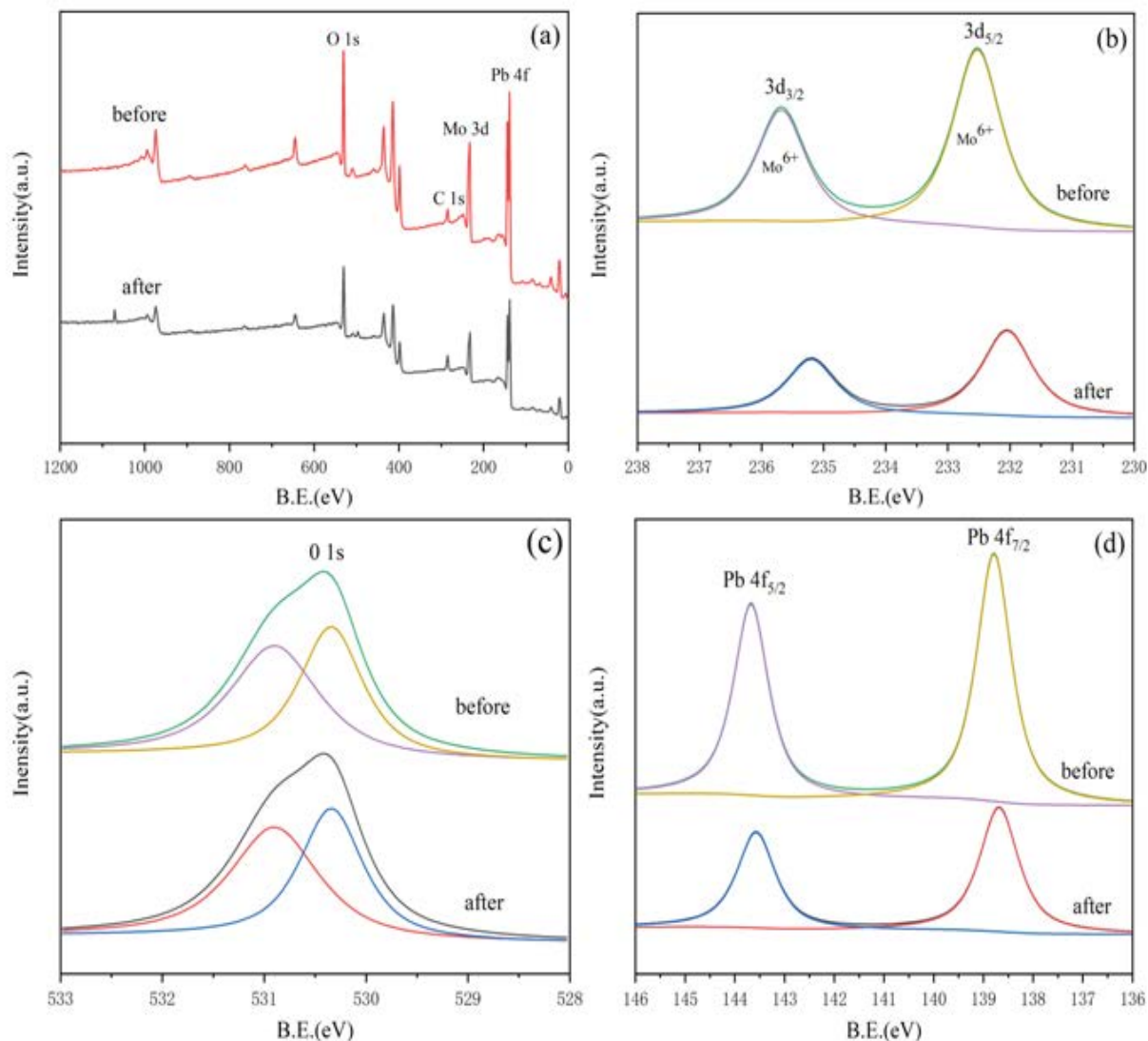


Fig. 3. XPS spectra of the catalyst before and after used five times: (a) survey spectrum of the sample, (b) Mo 3d, (c) O 1s, and (d) Pb 4f.

degrade organic contaminants was the effective separation of holes and photoelectrons. The interfacial charge transfer dynamics of the 2D PbMoO_4 was evaluated by employing the photocurrent-time measurement (Fig. 6). As displayed by Fig. 6, 2D PbMoO_4 could produce transient photocurrent responses obviously. And when the light turned on, the photocurrent intensity kept at a relatively high value. However, when the light turned off the value rapidly decreased to zero. The results indicated that 2D PbMoO_4 had a strong ability in charge separation.

3.2. Effects of adsorption and photodegradation

It was meaningful to study the effects of light conditions and adsorption for the photocatalytic efficiency. As shown in Fig. 7, the photocatalytic degradation efficiency of TC was 74% in the TC and 2D PbMoO_4 mixed solution and xenon lamp systems. The concentration of TC in the TC and 2D PbMoO_4 mixed solution did not change after 120 min under

dark conditions, indicating that 2D PbMoO_4 will not adsorb TC. In addition, the concentration of TC in the TC solution and xenon lamp systems did not change significantly after 120 min under the irradiation of visible light, indicating that TC could not be degraded by visible light. The above results validated that the effects of adsorption and photodegradation on the photocatalytic degradation of TC could be excluded, thus providing higher accuracy for the experimental data.

3.3. Influence of 2D PbMoO_4 dosage on the TC degradation

The effect of 2D PbMoO_4 dosage on TC degradation in the scope of 30 to 150 mg L^{-1} was investigated. Fig. 8a reveals that the degradation efficiency enhanced with increase of the photocatalyst dosage till the peak (about 95%) appeared at around 90 mg L^{-1} and then began to reduce. The improvement of TC removal was benefited from the rise in active sites raised by the amount of the catalyst [32].

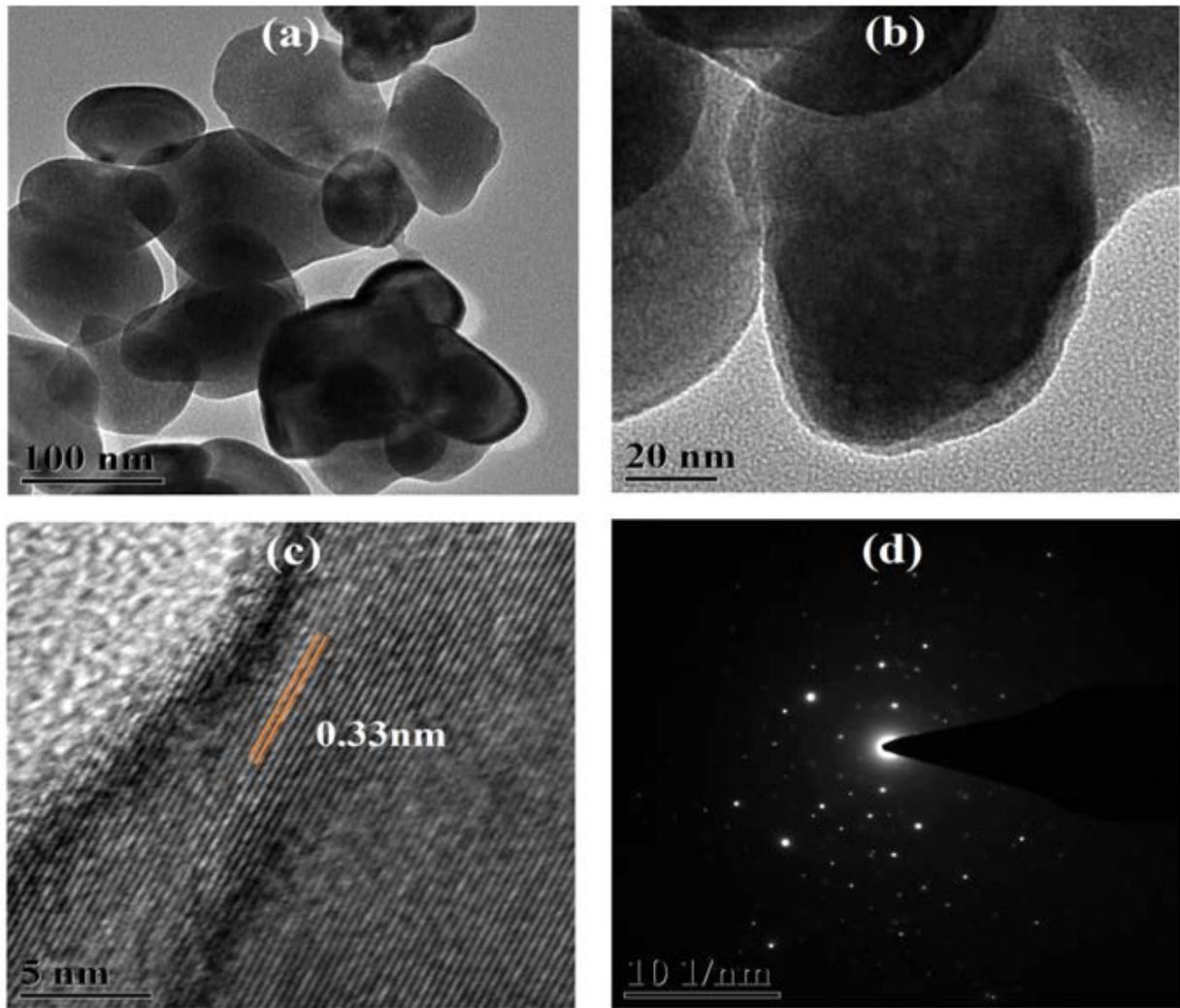


Fig. 4. TEM characterization of 2D PbMoO_4 : (a and b) High and low magnification, (c) lattice fringe spacing and (d) electron diffraction.

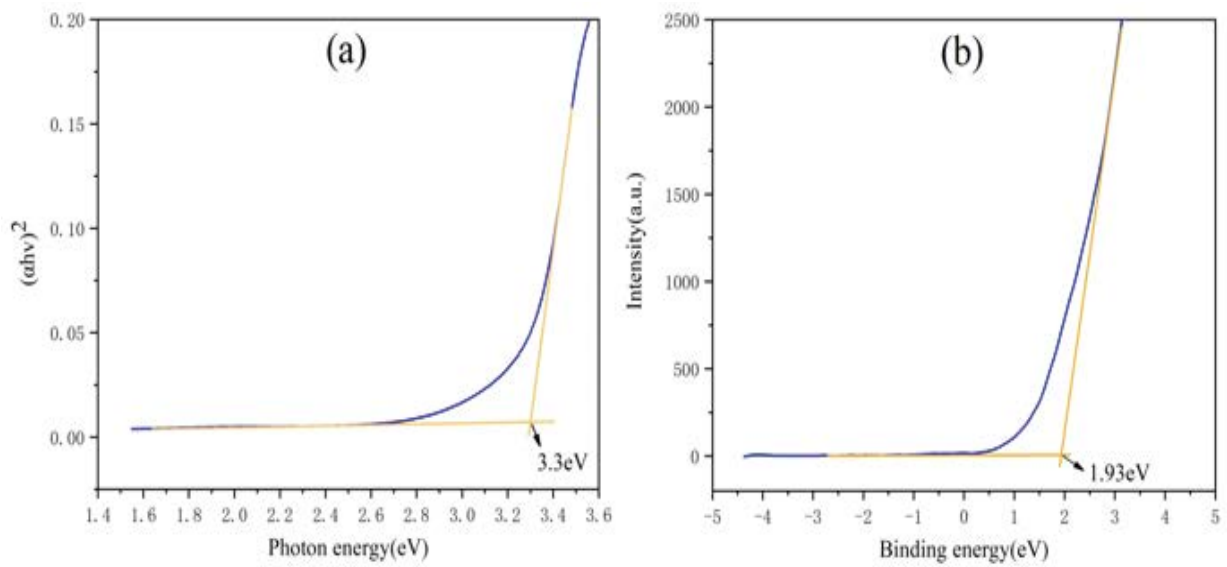


Fig. 5. (a) Tauc plot of 2D PbMoO_4 and (b) the XPS valence graphs of 2D PbMoO_4 nanosheets.

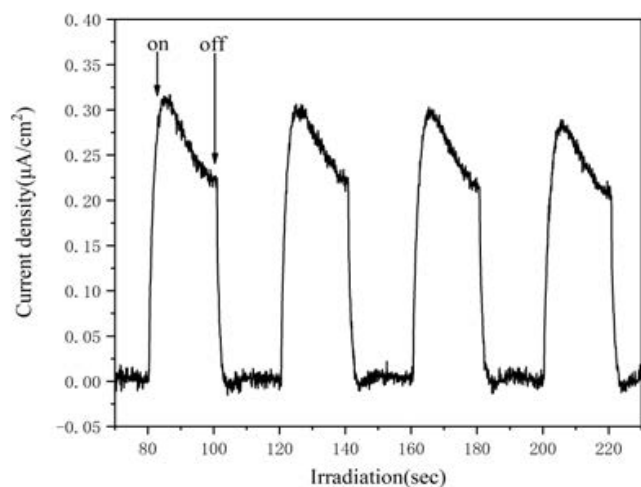


Fig. 6. Transient photocurrent responses of the 2D PbMoO₄.

However, the degradation efficiency of TC was reduced due to the agglomeration of the catalyst and the scattering of light, when the catalyst dosage was too high. The agglomeration could not only decline the available catalyst surface for photon absorption but also decrease the active sites of the catalysts [33]. The reductive effect of light could promote sedimentation or dispersion of light thus reduced the availability of light [34].

3.4. Effect of initial pH value on the TC degradation

The pH value of aqueous solution usually played an important role in TC photocatalytic degradation, as it had a strong influence on the surface property of photocatalyst and the stability of TC. As depicted in Fig. 8b, when pH increased, the degradation rate increased and then decreased, the highest TC degradation was (95%) at pH = 9.0. On one hand, it was reported that TC was more stable in acidic conditions than in alkaline conditions [35,36]. On the other hand, the pH value of the solution could largely affect the surface property of photocatalyst and control the surface charge. When pH lower or higher catalyst's pH_{pzc} , it would protonate or deprotonate, which had an association of the adsorption of TC [37]. According to reported literature, the reactive species that degraded TC in solution was strongly influenced by OH⁻ [38]. As proposed by Wang [33], the production of OH[•] on 2D PbMoO₄ was enhanced by OH⁻. Integrating the above analyses, the increase of pH value in solution would improve the generation of OH[•], accelerating the degradation of TC. While pH continued to increase, some chromogenic products were produced during the degradation, which inhibited the transmittance of sunlight thus decreased the degradation efficiency [39].

3.5. Influence of initial TC concentration on TC degradation

The effect of initial TC concentration on the TC degradation was evaluated. As shown in Fig. 8c, the degradation rate declined with the increase of initial TC concentration. After being irradiated for 120 min, 97.1%, 95.2%, 94%, 90%

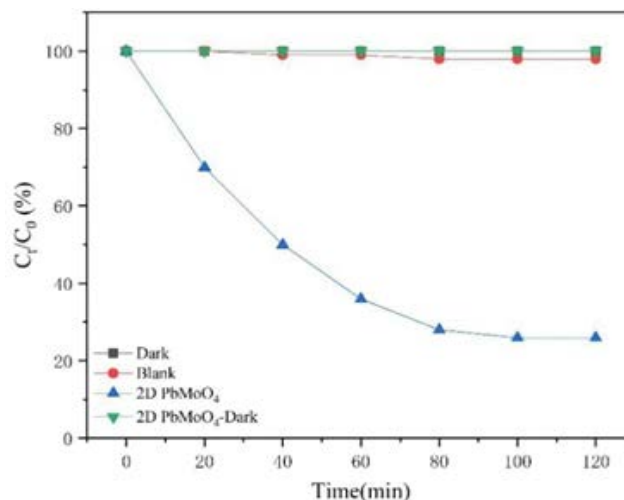


Fig. 7. Degradation of TC under different conditions.

and 86% of TC were degraded in the solution with the initial concentrations of 50, 100, 150, 200 and 250 mg L⁻¹, respectively. It was well known that at low substrate concentration, the photolytic reaction was controlled by the kinetic regime, but at high concentration, the process was controlled by mass transfer lowering the reaction rate. In addition, in high initial TC concentration solution, TC molecules would absorb photons, hindering the arrival of photons to the photocatalyst surface [40], as well as increase the internal optical density, preventing light from passing through the solution [41], resulting in a decline in photocatalytic rate. Moreover, in higher initial TC concentration solution, more TC molecules were adsorbed on the surface of the catalyst, leading to the lack of any direct contact between TC molecules and OH[•] or h⁺, thus prevented the reaction between them. The above results also could be owed to the fact that in all solutions, the number of reactive radicals generated was equal under the same conditions. Therefore, at lower TC concentrations TC molecules were a trend to react with radicals. These results were similar to those obtained by Chen et al. [42] and Ahmadi et al. [43], who concluded that with visible-light irradiation the TC photocatalytic removal rate decreased with the increase of TC initial concentration.

3.6. Identification of reactive species

In order to identify the reactive species during the photocatalytic degradation and investigate the corresponding photocatalytic mechanism, EDTA, IPA and PBQ were applied as the scavengers of h⁺, OH[•] and O₂^{-•}, respectively. As depicted in Fig. 8d, when PBQ was added to the solution, the TC degradation rate was significantly depressed revealing that a great amount of O₂^{-•} were participated in the TC degradation processes. After IPA was added to the solution, the photocatalytic degradation efficiency of TC did not change significantly, indicating that OH[•] plays an unimportant role during the TC degradation process. When EDTA-2Na was added to the solution, the photocatalytic degradation efficiency of 2D PbMoO₄ to TC was 58%. Thus, the trapping experiments illustrated that

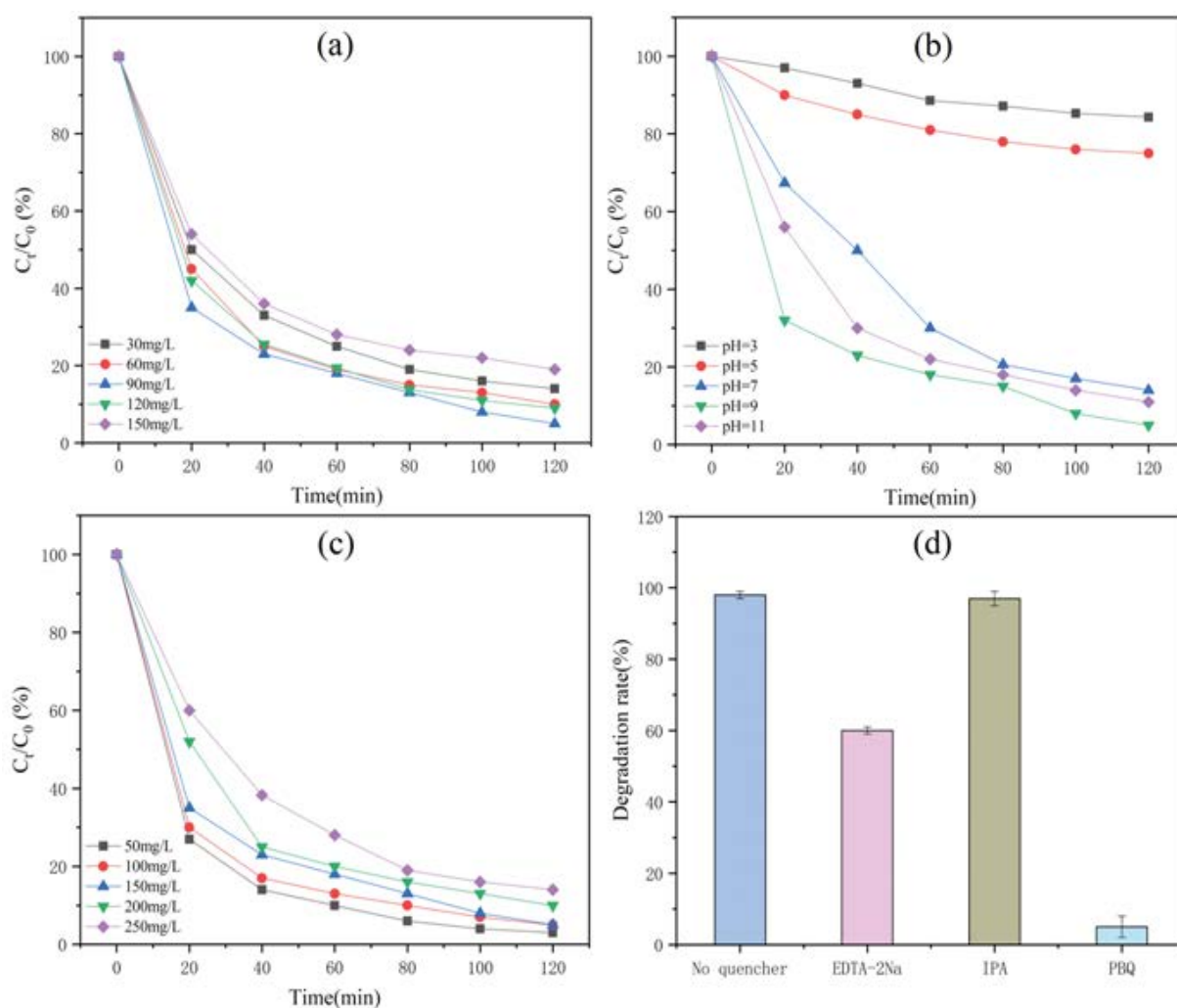
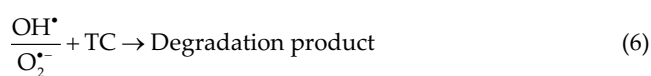
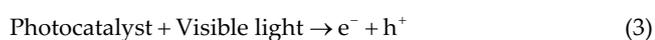


Fig. 8. Effect of reaction conditions on the removal efficiency of TC (a) the dosage of 2D PbMoO₄ ([TC] = 150 mg L⁻¹; pH 9; lamp power: 300 W), (b) initial pH ([TC] = 150 mg L⁻¹; [PbMoO₄] = 90 mg L⁻¹; lamp power: 300 W), (c) initial TC concentration ([PbMoO₄] = 90 mg L⁻¹; pH 9; lamp power: 300 W), and (d) quencher ([TC] = 150 mg L⁻¹; [PbMoO₄] = 90 mg L⁻¹; pH 9; lamp power: 300 W).

O₂^{•-}, OH[•] and h⁺ each could contribute to TC photocatalytic degradation and O₂^{•-} played the most important role in the process. It was known that the major procedure of photocatalytic reaction occurred on the surface of photocatalyst [44]. The surface of 2D PbMoO₄ would produce e⁻ and h⁺ when excited with visible light. Subsequently, the O₂ adsorbed on the surface of 2D PbMoO₄ captured the excited electrons thus O₂^{•-} yielded, which was the main oxidizing species to degrade TC [45]. These conclusions were well agreed with the results obtained from the active species trapping experiment. Based on the above results the process of TC photocatalytic degradation could be written as follows:



3.7. Preliminary analysis of possible pathways for tetracycline degradation

It was meaningful to understand the degradation pathway of 2D PbMoO₄ photocatalytic degradation of tetracycline. The intermediate product of TC was analyzed by LC-MS. The MS spectrum and possible structural information were shown in Fig. S1. According to the results of LC-MS and previous literature, the possible degradation pathway of 2D PbMoO₄ photocatalytic degradation of TC was proposed as illustrated in Fig. 9. TC could be transformed to TC 1 (m/z = 461) and TC 2 (m/z = 477) by hydroxylation process [21]. Furthermore, TC 1 might be oxidized to form the quinone products with TC 3 and TC 4 (m/z = 415) [46]. Similarly, it had been reported that original TC molecules could lose the N-methyl group to generate TC 5 (m/z = 417). TC 5 was continuously attacked by active

radicals and changed to TC 6 ($m/z = 374$, not detected in this study). Because of the strong oxidizing active species, the carboatomic ring in TC 6 could be cleavage to generate TC 7 ($m/z = 277$) [47]. On the other hand, TC 8 ($m/z = 427$) could be formed by the dehydration of TC [48]. The generation of TC 9 ($m/z = 362$) could be ascribed to the acylamino and the loss of the *N*-methyl group in TC 8. And the TC 10 ($m/z = 318$) arose from TC 9 which through a ring-opening reaction [49]. Accompanied by the continuous effect of active species, TC 10 could be further oxidized to TC 11 ($m/z = 274$). In brief, the above transformation intermediates were eventually be oxidized into CO_2 and H_2O .

3.8. Stability and recyclability

The stability and reusability of 2D PbMoO_4 photocatalyst were essential to make the degradation more economical. The reusability of 2D PbMoO_4 was examined by repeating the TC photocatalytic degradation for five consecutive cycles (Fig. 9). After five cycle experiments, the catalyst still possessed a high photocatalytic activity for TC degradation, and the degradation rate was 95%, only reduced 1%, manifesting the catalyst had excellent stability. The stability of the photocatalyst was further confirmed by the XRD pattern (Fig. 2) and XPS spectra (Fig. 3) of the used 2D PbMoO_4 (five times). Figs. 2 and 3 demonstrate

that the XRD patterns and XPS spectra of the recycled 2D PbMoO_4 were very similar to those of original 2D PbMoO_4 before reaction. In addition, a slight shifting of Pb 4f peaks was found after recycling suggested there were a very small amount of Pb^{2+} was generated on the surface of the catalyst. The above results indicated that 2D PbMoO_4 holds extraordinary stability for the degradation of TC.

3.9. Effect of different water matrix on TC degradation

In order to evaluate the effect of different water matrix on 2D PbMoO_4 photocatalytic degradation of TC, four different water were conducted experiments. As shown in Fig. 10, among different initial TC concentrations in the same water matrix, the low-concentration TC solution had the highest degradation efficiency. The degradation efficiency of TC in different water matrices: $\text{UW} > \text{AW} > \text{FW} > \text{MW}$. Despite the different water matrix, 2D PbMoO_4 still exhibited higher photocatalytic degradation activity. When the TC concentration in the four different water substrates was 50 mg L^{-1} , it showed good degradation effect, and the removal rates were 96%, 94%, 91% and 88%, respectively.

TC had the highest photocatalytic degradation efficiency in UW. On the one hand, it is due to less suspended solid particles in the solution. On the other hand, no impurities affected the activity of the photocatalytic material in the

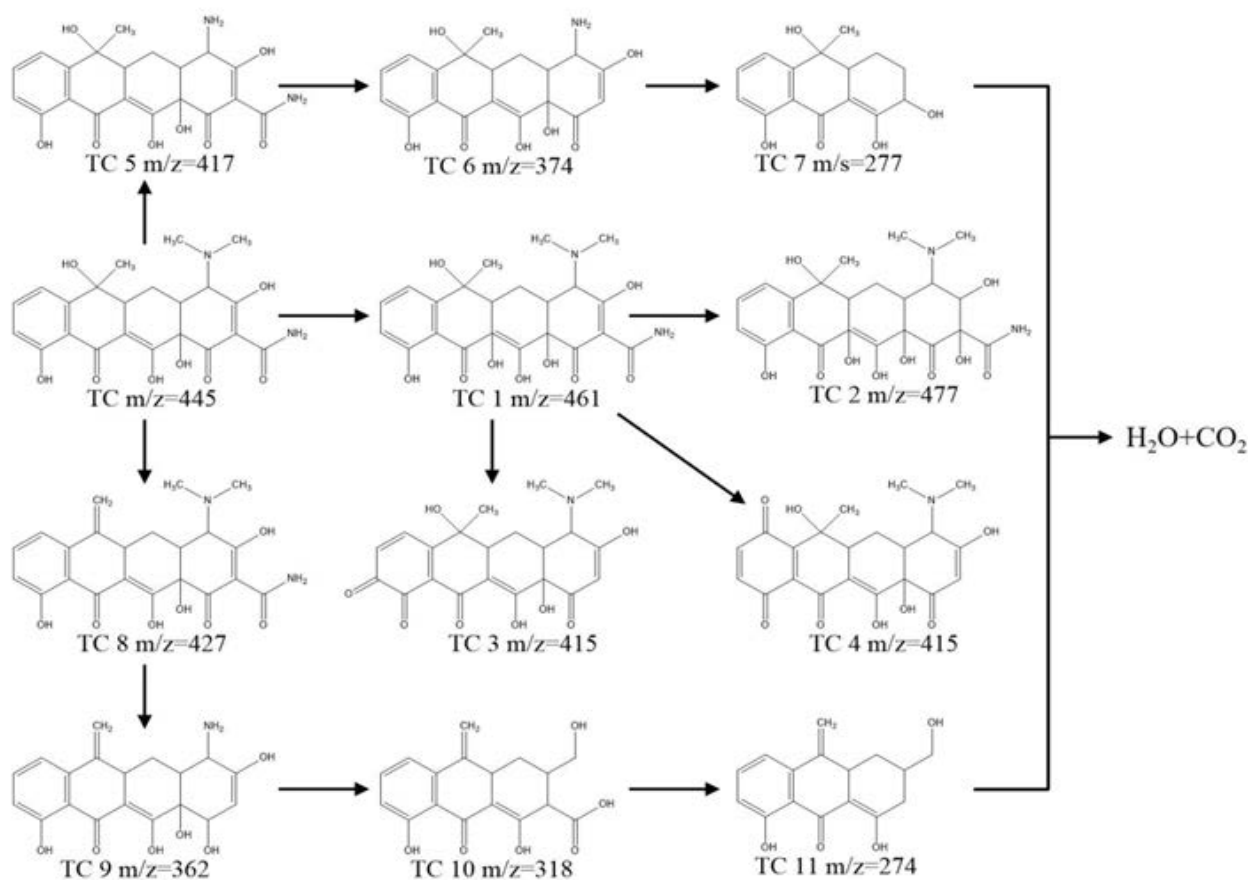


Fig. 9. Proposed degradation pathway of TC.

solution. In addition, the organic carbon, organic nitrogen, NO_3^- , PO_4^- and NH_4^+ present in AW could react with active species and inhibit the photocatalytic degradation of TC [50]. The reduction of the efficiency of photocatalytic degradation of TC in FW was mainly due to the high concentration of chemical oxygen demand, ammonia nitrogen concentration and total phosphorus concentration [51]. Similarly, the characteristics of MW were a mainly dark color, turbidity, high content of organic matter and inorganic salts, etc. The visible light reaching the surface of the photocatalyst could be reduced in dark and turbid sewage. High concentrations of organic matter may compete for active species with TC, which would reduce the photocatalytic degradation efficiency of TC [52]. There had more types of inorganic anions and inorganic cations in MW than the above sewage, and most of the anions can act as quenchers. The inorganic cations in MW would change the inherent viscoelasticity of nonionic and ionic surfactants at the interface

between catalyst surface and bulk solution, thus affecting the adsorption of pollutants [53].

3.10. Kinetic study of TC degradation by 2D PbMoO_4

To assess the effect of the different water matrix on TC degradation, experiments were carried out four with different water matrices, that is, UW, AW, FW, and MW (Fig. 10). Although the water matrix was different 2D PbMoO_4 displayed the highest activity when TC concentration was 50 mg L^{-1} . The removal rate of TC in UW, AW, FW, and MW were 96%, 94%, 91%, and 88%, respectively. The Kinetic study for TC photocatalytic degradation in the indifferent matrix was acquired through the pseudo-first-order kinetic model, which was written as follow:

$$-\ln \frac{C_t}{C_0} = k_t t \quad (7)$$

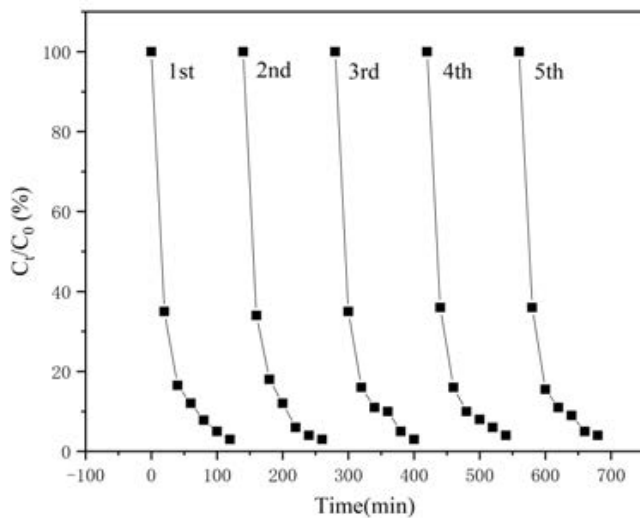


Fig. 10. Cycling runs for TC degradation with 2D PbMoO_4 .

where t was a time (min), k was the degradation kinetic constant (min^{-1}), C_0 was the initial TC concentration (mg L^{-1}), and C_t was the concentration of TC at time t (mg L^{-1}). The relevant results of the analysis are stated in Table 1. According to the calculated regression coefficient (R^2), the degradation process followed the pseudo-first-order kinetic model well. Degradation of UW exhibited the highest rate constant (0.01977 min^{-1}) followed by AW (0.01706 min^{-1}), FW (0.01543 min^{-1}) and MW (0.01367 min^{-1}) when TC concentration was 50 mg L^{-1} .

3.11. Summary of photocatalytic degradation performance of lead molybdate

A comparison between the degradation performance of 2D PbMoO_4 nanosheets observed in this work and a selection of previous reports on lead molybdates with different morphologies are summarized in Table 2. As demonstrated in the table, higher catalysts dosages in most of the reported, which was not suitable for large-scale applications

Table 1
Analysis different water matrices on the kinetic of TC degradation

Water matrix	TC (mg L^{-1})	Regression equation	k_0 (min^{-1})	R^2	$t_{1/2}$ (min)
UW	50	$y = 0.01977x + 0.83267$	1.977×10^{-2}	0.99447	35.05
	100	$y = 0.018x + 0.69$	1.8×10^{-2}	0.95005	38.50
	150	$y = 0.01727x + 0.446$	1.727×10^{-2}	0.96745	40.13
AW	50	$y = 0.01706x + 0.67933$	1.706×10^{-2}	0.97692	40.62
	100	$y = 0.01573x + 0.53733$	1.573×10^{-2}	0.98069	44.06
	150	$y = 0.01463x + 0.47933$	1.463×10^{-2}	0.97854	47.37
FW	50	$y = 0.01543x + 0.55$	1.543×10^{-2}	0.99692	44.91
	100	$y = 0.01446x + 0.47467$	1.446×10^{-2}	0.99585	47.93
	150	$y = 0.0132x + 0.44187$	1.32×10^{-2}	0.99285	52.50
MW	50	$y = 0.01367x + 0.498$	1.367×10^{-2}	0.98584	50.69
	100	$y = 0.0129x + 0.442$	1.29×10^{-2}	0.99351	53.72
	150	$y = 0.01196x + 0.36133$	1.196×10^{-2}	0.9937	57.94

$$t_{1/2} = 0.693/k_0$$

Table 2
Summary of photocatalytic degradation performance of different morphology of PbMoO₄

Morphology	Target	Recommended operating conditions	Degradation effect	References
Dendritic nanostructures	RhB 4.43 mg L ⁻¹	0.5 g L ⁻¹ ; 500 W Xe lamp	100%, 100 min	[54]
Nanoparticles coatings	TC 10 mg L ⁻¹	2.85 g L ⁻¹ ; 35 W Xe lamp	55%, 180 min	[55]
Spherical nanoparticles	RhB 10 mg L ⁻¹	1 g L ⁻¹ ; 300 W Xe lamp	90%, 120 min	[45]
Spherical nanoparticles	RhB 20 mg L ⁻¹	0.2 g L ⁻¹ ; Visible light	90%, 165 min	[56]
2D nanosheets	TC 150 mg L ⁻¹	0.09 g L ⁻¹ ; 300 W Xe lamp	90%, 120 min	Present work

in real life. Additionally, PbMoO₄ was only suitable for the photocatalytic degradation of low concentrations of pollutants in previous reports. In contrast, 2D nanosheets had a higher surface area and more reactive active sites on their surface, which significantly improves their photocatalytic activity. 2D morphology of PbMoO₄ had the advantages of high efficiency and low dosage for photocatalytic degradation and was very suitable for the treatment of TC in sewage. This shows the superiority and importance of 2D PbMoO₄ nanosheets in the photocatalytic degradation of organic pollutants, compared with other nanomorphology of this crystal.

4. Conclusion

The no-layer 2D PbMoO₄ had been successfully synthesized and applied for the degradation of TC in UW, AW, FW and MW under simulated solar irradiation. TC (50–150 mg L⁻¹) was almost eliminated in 120 min. TC degradation rate was improved by the increase of the catalyst dosage when it was lower than 90 mg L⁻¹ and decreased when the usage was above that. The photocatalytic process was pH-dependent, and the most favorable pH value was 9. 2D PbMoO₄ was appropriate for photodegradation of TC in water, especially at low TC concentration. In the photocatalytic process, O₂^{•-} radicals played a leading role in the degradation of TC. 2D PbMoO₄ had excellent stability even after five successive runs. In summary, 2D PbMoO₄ was a promising photocatalyst for oxidation technology in water/wastewater treatment due to its applicability in high degradation efficiency, catalyst stability, and reusability. It could be employed as a post approach in conventional wastewater treatment to reach the reuse of the water as it could efficiently remove contaminants, and consequently prevents them from entering the environment.

Acknowledgments

This work was supported in part by the Research Foundation of Education Bureau of Hunan Province (No. 19A509); Natural Science Foundation of Hunan province (No. 2018JJ2675); Major Science and Technology Program of Hunan province (No. 2017NK1014); Key Technology R&D Program of Hunan Province (No. 2016TP2007, 2016TP1014).

References

- [1] S. Coenen, N. Adriaenssens, A. Versporten, A. Muller, G. Minalu, C. Faes, European surveillance of antimicrobial consumption

- (ESAC): outpatient use of tetracyclines, sulphonamides and trimethoprim, and other antibacterials in Europe, *J. Antimicrob. Chemother.*, 66 (2011) 57–70.
- [2] Q.W. Chen, X. Guo, G.F. Hua, G.L. Li, R.R. Feng, X.L. Liu, Migration and degradation of swine farm tetracyclines at the river catchment scale: can the multi-pond system mitigate pollution risk to receiving rivers?, *Environ. Pollut.*, 220 (2017) 1301–1310.
- [3] K. Chen, J.L. Zhou, Occurrence and behavior of antibiotics in water and sediments from the Huangpu River, Shanghai, China, *Chemosphere*, 95 (2014) 604–612.
- [4] Y.M. Chen, K.S.-Y. Leung, J.W.-C. Wong, A. Selvam, Preliminary occurrence studies of antibiotic residues in Hong Kong and Pearl River Delta, *Environ. Monit. Assess.*, 185 (2013) 745–754.
- [5] L.A.T. Cox Jr., D.A. Popken, Assessing potential human health hazards and benefits from subtherapeutic antibiotics in the United States: tetracyclines as a case study, *Risk Anal.*, 30 (2010) 432–457.
- [6] J. Allahbakhsh, M. Alireza, N. Simin, H.M. Amir, A. Mahmood, G. Hamed, Assessment of tetracycline contamination in surface and groundwater resources proximal to animal farming houses in Tehran, Iran, *J. Environ. Health Sci.*, 14 (2016) 4.
- [7] W.W. Ben, J. Wang, R.K. Cao, M. Yang, Y. Zhang, Z.M. Qiang, Distribution of antibiotic resistance in the effluents of ten municipal wastewater treatment plants in China and the effect of treatment processes, *Chemosphere*, 172 (2017) 392–398.
- [8] D. Rydzynski, A.I. Piotrowicz-Cieslak, H. Grajek, D.J. Michalczyk, Instability of chlorophyll in yellow lupin seedlings grown in soil contaminated with ciprofloxacin and tetracycline, *Chemosphere*, 184 (2017) 62–73.
- [9] A.C. Thompson, P.P. Sikorowski, Effect of tetracycline hydrochloride on the physical and chemical properties of *Heliothis virescens* larvae, *Comp. Biochem. Physiol. C: Toxicol. Pharmacol.*, 79 (1984) 31–33.
- [10] C.S. Miller, G.J. Mcgarity, Tetracycline-induced renal failure after dental treatment, *J. Am. Dent. Assoc.*, 140 (2009) 56–60.
- [11] M.B. Simpson, J. Pryzbylik, S.B.B. Innis, M.A. Denham, Hemolytic anemia after tetracycline therapy, *N. Engl. J. Med.*, 312 (1985) 840–842.
- [12] N.J. O'Doherty, Acute benign intracranial hypertension in an infant receiving tetracycline, *Dev. Med. Child. Neurol.*, 7 (2008) 677–680.
- [13] N.P. Marathe, V.R. Regina, S.A. Walujkar, S.S. Charan, E.R.B. Moore, D.G. Joakim Larsson, Y.S. Shouche, A treatment plant receiving waste water from multiple bulk drug manufacturers is a reservoir for highly multi-drug resistant integron-bearing bacteria, *PLoS One*, 8 (2013) e77310, doi: 10.1371/journal.pone.0077310.
- [14] S. Aydin, B. Ince, O. Ince, Development of antibiotic resistance genes in microbial communities during long-term operation of anaerobic reactors in the treatment of pharmaceutical wastewater, *Water Res.*, 83 (2015) 337–344.
- [15] W.Y. Teoh, J.A. Scott, R. Amal, Progress in heterogeneous photocatalysis: from classical radical chemistry to engineering nanomaterials and solar reactors, *J. Phys. Chem. Lett.*, 3 (2012) 629–639.

- [16] M.N. Chong, B. Jin, C.W.K. Chow, C. Saint, Recent developments in photocatalytic water treatment technology: a review, *Water Res.*, 44 (2010) 2997–3027.
- [17] Y. Wu, N.F.Y. Tam, M.H. Wong, Effects of salinity on treatment of municipal wastewater by constructed mangrove wetland microcosms, *Mar. Pollut. Bull.*, 57 (2008) 727–734.
- [18] M.M.Y.A. Alsaif, M.R. Field, T. Daeneke, A.F. Chrimes, W. Zhang, B.J. Carey, K.J. Berean, S. Walia, J. van Embden, B. Zhang, K. Latham, K. Kalantar-Zadeh, J.Z. Ou, Exfoliation solvent dependent plasmon resonances in two-dimensional sub-stoichiometric molybdenum oxide nanoflakes, *ACS Appl. Mater. Interfaces*, 8 (2016) 3482.
- [19] N. Dhar, N. Syed, M. Mohiuddin, A. Jannat, A. Zavabeti, B.Y. Zhang, R.S. Datta, P. Atkin, N. Mahmood, D. Esrafilzadeh, T. Daeneke, K. Kalantar-Zadeh, Exfoliation behavior of van der Waals strings: case study of Bi_2S_3 , *ACS Appl. Mater. Interfaces*, 10 (2018) 42603–42611.
- [20] D.-A. Jia, D.-M. Zhou, Y.-J. Wang, H.-W. Zhu, J.-L. Chen, Adsorption and cosorption of Cu(II) and tetracycline on two soils with different characteristics, *Geoderma*, 146 (2008) 224–230.
- [21] W.J. Wang, P. Xu, M. Chen, G.M. Zeng, C. Zhang, C.Y. Zhou, Y. Yang, D.L. Huang, C. Lai, M. Cheng, L. Hu, W.P. Xiong, H. Guo, M. Zhou, Alkali metal-assisted synthesis of graphite carbon nitride with tunable band-gap for enhanced visible-light-driven photocatalytic performance, *ACS Sustainable Chem. Eng.*, 6 (2019) 15503–15516.
- [22] Y. Yang, C. Zhang, D.L. Huang, G.M. Zeng, J.H. Huang, C. Lai, C.Y. Zhou, W.J. Wang, H. Guo, W.J. Xue, R. Deng, M. Cheng, W.P. Xiong, Boron nitride quantum dots decorated ultrathin porous $\text{g-C}_3\text{N}_4$: intensified exciton dissociation and charge transfer for promoting visible-light-driven molecular oxygen activation, *Appl. Catal., B*, 245 (2019) 87–99.
- [23] F. Haque, A. Zavabeti, B.Y. Zhang, R.S. Datta, Y.F. Yin, Z.F. Yi, Y.C. Wang, N. Mahmood, N. Pillai, N. Syed, H. Khan, A. Jannat, N. Wang, N. Medhekar, K. Kalantar-Zadeh, J.Z. Ou, Ordered intracrystalline pores in planar molybdenum oxide for enhanced alkaline hydrogen evolution, *J. Mater. Chem. A*, 7 (2019) 257–268.
- [24] A. Zavabeti, B.Y. Zhang, I.A. de Castro, J.Z. Ou, B.J. Carey, M. Mohiuddin, R. Datta, C.L. Xu, A.P. Mouritz, C.F. McConville, A.P. O'Mullane, T. Daeneke, K. Kalantar-Zadeh, Green synthesis of low-dimensional aluminum oxide hydroxide and oxide using liquid metal reaction media: ultrahigh flux membranes, *Adv. Funct. Mater.*, 28 (2018) 1804057.1–1804057.9.
- [25] W.K. Wong-Ng, H.F. McMurdie, C.R. Hubbard, A.D. Mighell, JCPDS-ICDD research associateship (cooperative program with NBS/NIST), *J. Res. Natl. Inst. Stan.*, 106 (2001) 1013.
- [26] M.R.D. Bomio, L.S. Cavalcante, M.A.P. Almeida, R.L. Tranquilin, N.C. Batista, P.S. Pizani, M.S. Li, J. Andres, E. Longo, Structural refinement, growth mechanism, infrared/Raman spectroscopies and photoluminescence properties of PbMoO_4 crystals, *Polyhedron*, 50 (2013a) 532–545.
- [27] K. Dai, Y. Yao, H. Liu, I. Mohamed, H. Chen, Q.Y. Huang, Enhancing the photocatalytic activity of lead molybdate by modifying with fullerene, *J. Mol. Catal. A: Chem.*, 374–375 (2013) 111–117.
- [28] L.R. Pederson, Two-dimensional chemical-state plot for lead using XPS, *J. Electron. Spectrosc.*, 28 (1982) 203–209.
- [29] K.S. Kim, T.J. O'Leary, N. Winograd, X-ray photoelectron spectra of lead oxides, *Anal. Chem.*, 45 (1973) 2214–2218.
- [30] W.M. Du, L.X. Liu, K.K. Zhou, X.D. Ma, Y.M. Hao, X.F. Qian, Black lead molybdate nanoparticles: facile synthesis and photocatalytic properties responding to visible light, *Appl. Surf. Sci.*, 328 (2015) 428–435.
- [31] R.S. Datta, J.Z. Ou, M. Mohiuddin, B.J. Carey, B.Y. Zhang, H. Khan, N. Syed, A. Zavabeti, F. Haque, T. Daeneke, K. Kalantar-Zadeh, Two dimensional PbMoO_4 : a photocatalytic material derived from a naturally non-layered crystal, *Nano Energy*, 49 (2018b) 237–246.
- [32] G.H. Safari, M. Hoseini, M. Seyed-Salehi, H. Kamani, J. Jaafari, A.H. Mahvi, Photocatalytic degradation of tetracycline using nanosized titanium dioxide in aqueous solution, *Int. J. Environ. Sci. Technol.*, 12 (2015) 603–616.
- [33] P.H. Wang, P.-S. Yap, T.-T. Lim, C.-N.-S. tridoped TiO_2 for photocatalytic degradation of tetracycline under visible-light irradiation, *Appl. Catal., A*, 399 (2011) 252–261.
- [34] R. Nosrati, A. Olad, R. Maramifar, Degradation of ampicillin antibiotic in aqueous solution by ZnO/polyaniline nanocomposite as photocatalyst under sunlight irradiation, *Environ. Sci. Pollut. Res.*, 19 (2012) 2291–2299.
- [35] J.R.D. McCormick, S.M. Fox, L.L. Smith, B.A. Bitler, J. Reichenthal, V.E. Origoni, W.H. Muller, R. Winterbottom, A.P. Doerschuk, Studies of the reversible epimerization occurring in the tetracycline family. The preparation, properties and proof of structure of some 4-epi-tetracyclines, *J. Am. Chem. Soc.*, 79 (1957) 2849–2858.
- [36] C.R. Stephens, K. Murai, K.J. Brunings, R.B. Woodward, Acidity constants of the tetracycline antibiotics, *J. Am. Chem. Soc.*, 78 (1956) 4155–4158.
- [37] H.A. Hamad, W.A. Sadik, M.M. Abd El-Latif, A.B. Kashyout, M.Y. Feteha, Photocatalytic parameters and kinetic study for degradation of dichlorophenol-indophenol (DCPIP) dye using highly active mesoporous TiO_2 nanoparticles, *J. Environ. Sci.*, 43 (2016) 26–39.
- [38] X.-D. Zhu, Y.-J. Wang, R.-J. Sun, D.-M. Zhou, Photocatalytic degradation of tetracycline in aqueous solution by nanosized TiO_2 , *Chemosphere*, 92 (2013) 925–932.
- [39] I. Dalmázio, M.O. Almeida, R. Augusti, T.M.A. Alves, Monitoring the degradation of tetracycline by ozone in aqueous medium via atmospheric pressure ionization mass spectrometry, *J. Am. Soc. Mass. Spectrom.*, 18 (2007) 679–687.
- [40] R. Mohammadi, B. Massoumi, M. Rabani, Photocatalytic decomposition of amoxicillin trihydrate antibiotic in aqueous solutions under UV irradiation using Sn/TiO_2 nanoparticles, *Int. J. Photoenergy*, 2012 (2012) 1–11, <https://doi.org/10.1155/2012/514856>.
- [41] B. Jung, A. Safan, Y.H. Duan, V. Kaushik, B. Batchelor, A. Abdel-Wahab, Removal of arsenite by reductive precipitation in dithionite solution activated by UV light, *J. Environ. Sci.*, 74 (2018) 171–179.
- [42] Y. Chen, H. Li, Z.P. Wang, T. Tao, C. Hu, Photoproducts of tetracycline and oxytetracycline involving self-sensitized oxidation in aqueous solutions: effects of Ca^{2+} and Mg^{2+} , *J. Environ. Sci.*, 23 (2011) 1634–1639.
- [43] M. Ahmadi, H.R. Motlagh, N. Jaafarzadeh, A. Mostoufi, R. Saeedi, G. Barzegar, S. Jorfi, Enhanced photocatalytic degradation of tetracycline and real pharmaceutical wastewater using MWCNT/TiO_2 nano-composite, *J. Environ. Manage.*, 186 (2017) 55–63.
- [44] X.F. Chang, J. Huang, C. Cheng, W. Sha, X. Li, G.B. Ji, S.B. Deng, G. Yu, Photocatalytic decomposition of 4-*t*-octylphenol over NaBiO_3 driven by visible light: catalytic kinetics and corrosion products characterization, *J. Hazard. Mater.*, 173 (2010) 765–772.
- [45] W.Y. Jung, G.D. Lee, K.T. Lim, M.S. Lee, S.-S. Hong, Synthesis of PbMoO_4 nanoparticles using a facile surfactant-assisted microwave process and their photocatalytic activity, *J. Nanosci. Nanotechnol.*, 17 (2017) 2751–2755.
- [46] J. Wu, H. Zhang, N. Oturan, Y. Wang, L. Chen, M.A. Oturan, Application of response surface methodology to the removal of the antibiotic tetracycline by electrochemical process using carbon-felt cathode and DSA ($\text{Ti/RuO}_2\text{-IrO}_2$) anode, *Chemosphere*, 74 (2012) 614–620.
- [47] H. Guo, C.-G. Niu, L. Zhang, X.-J. Wen, C. Liang, X.-G. Zhang, D.-L. Guan, N. Tang, G.-M. Zeng, Construction of direct Z-scheme $\text{AgI/Bi}_2\text{Sn}_2\text{O}_7$ nanojunction system with enhanced photocatalytic activity: accelerated interfacial charge transfer induced efficient Cr(VI) reduction, tetracycline degradation and *Escherichia coli* inactivation, *ACS Sustainable Chem. Eng.*, 6 (2018) 8003–8016.
- [48] J. Cao, Z.-H. Yang, W.-P. Xiong, Y.-Y. Zhou, Y.-R. Peng, X. Li, C.-Y. Zhou, R. Xu, Y.-R. Zhang, One-step synthesis of Co-doped UiO-66 nanoparticle with enhanced removal efficiency of

- tetracycline: simultaneous adsorption and photocatalysis, *Chem. Eng. J.*, 353 (2018) 126–137.
- [49] H.R. Dong, Z. Jiang, C. Zhang, J.M. Deng, K.J. Hou, Y.J. Cheng, L.H. Zhang, G.M. Zeng, Removal of tetracycline by Fe/Ni bimetallic nanoparticles in aqueous solution, *J. Colloid Interface Sci.*, 513 (2018) 117–125.
- [50] L. Tang, J.J. Wang, G.M. Zeng, Y.N. Liu, Y.C. Deng, Y.Y. Zhou, J. Tang, J.J. Wang, Z. Guo, Enhanced photocatalytic degradation of norfloxacin in aqueous Bi_2WO_6 dispersions containing nonionic surfactant under visible light irradiation, *J. Hazard. Mater.*, 306 (2016) 295–304.
- [51] Z.S. Liu, L.P. Xu, X.D. Liang, Z.H. Wang, H.M. Zhang, Control the pollution of pig farm's manure wastewater and resource to cultivate microalgae, *Adv. Mater. Res.*, 1015 (2014) 725–728.
- [52] A. Achilleos, E. Hapeshi, N.P. Xekoukoulotakis, D. Mantzavinos, D. Fatta-Kassinos, Factors affecting diclofenac decomposition in water by UV-A/ TiO_2 photocatalysis, *Chem. Eng. J.*, 161 (2010) 53–59.
- [53] A. Bonfillon, D. Langevin, Viscoelasticity of monolayers at oil-water interfaces, *Langmuir*, 9 (1993) 2172–2177.
- [54] M. Hashim, C.G. Hu, X. Wang, X.Y. Li, D.L. Guo, Synthesis and photocatalytic property of lead molybdate dendrites with exposed (0 0 1) facet, *Appl. Surf. Sci.*, 258 (2012) 5858–5862.
- [55] S. Obregón, D.B. Hernández-Uresti, A. Vázquez, D. Sánchez-Martínez, Electrophoretic deposition of PbMoO_4 nanoparticles for photocatalytic degradation of tetracycline, *Appl. Surf. Sci.*, 457 (2018) 501–507.
- [56] S. Ayni, M. Sabet, M. Salavati-Niasari, Synthesis and characterization of lead molybdate nanostructures with high photocatalytic activity via simple co-precipitation method, *J. Cluster Sci.*, 27 (2015) 1–12.

Supplementary information

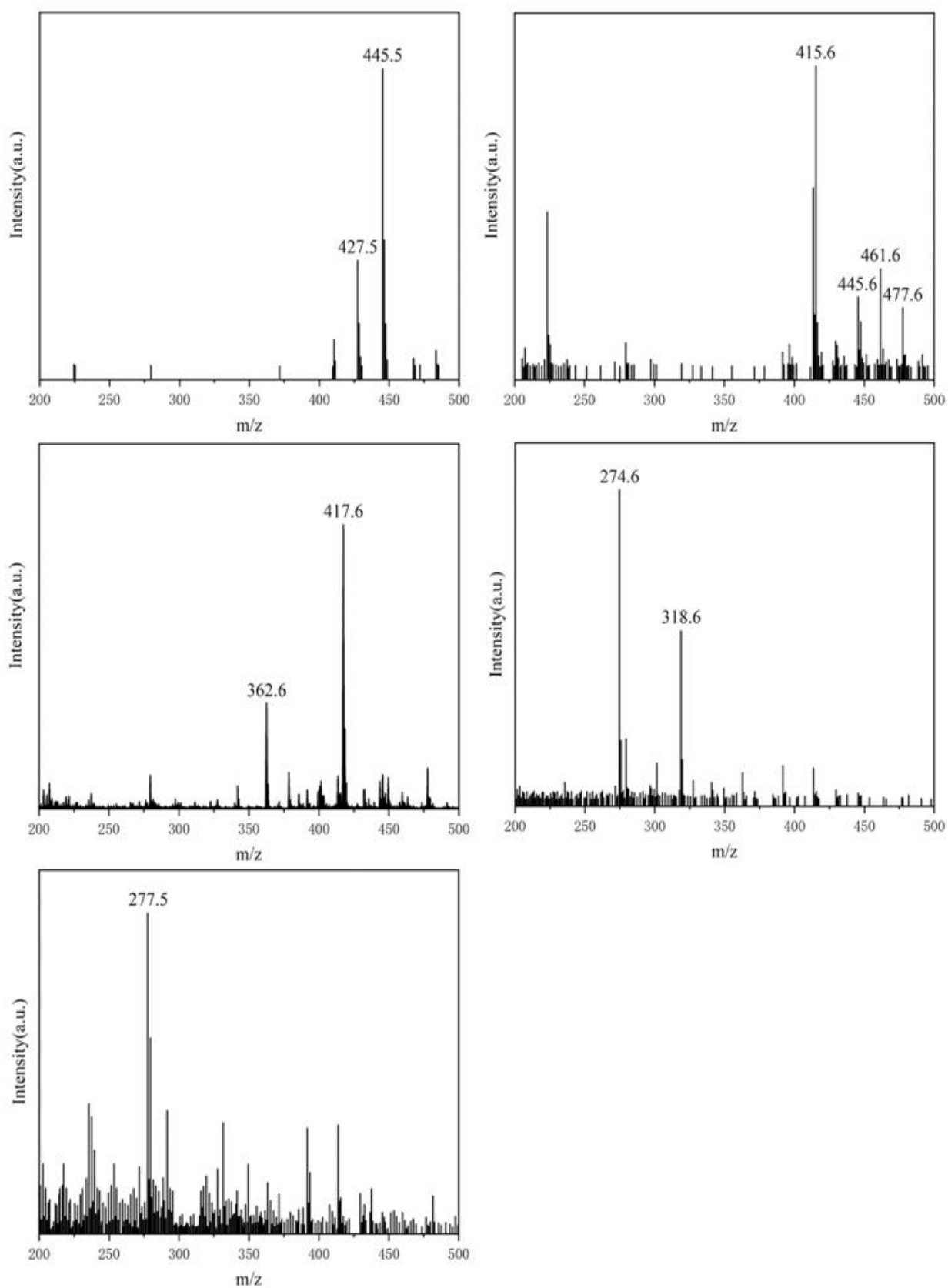


Fig. S1. MS spectra of the TC and possible intermediates.